The Southern Solar-type, Totally Eclipsing Binary PY Aquarii

Ronald G. Samec
Faculty Research Associate, Pisgah Astronomical Research Institute, 1 PARI Drive, Rosman, NC 28772; ronaldsamec@gmail.com

Heather A. Chamberlain
Pisgah Astronomical Research Institute, 1 PARI Drive, Rosman, NC 28772

Walter Van Hamme
Department of Physics, Florida International University, Miami, FL 33199

Received December 12, 2018; revised January 21, 2019; accepted January 24, 2019

Abstract We obtained new *BVRI* (Bessell) observations of the solar-type eclipsing binary PY Aqr in 2017 with the 0.6-m SARA South reflector located at Cerro Tololo Inter-American Observatory. A simultaneous Wilson-Devinney solution of the new 2017 light curves, the 2003 discovery curve, and the 2001–2009 ASAS light curve reveals a system configuration with a modest degree of over-contact (fill-out ≈ 18%) and total eclipses (duration ≈ 23 minutes). The photometrically determined mass ratio is ≈ 0.32. The temperature difference between the components is ≈ 130K, indicating two stars in reasonably good thermal contact. Light curve asymmetries are modeled with a cool spot region on the primary, more massive star. Spanning a 16-year time base, the light curves indicate a 0.049 ± 0.005 s/yr steady increase of the orbit period. This dp/dt is not unusual as compared to the unpublished poster paper at the 2018 IAU GA study of over 200 solar type binaries. Two methods were used in conducting the period study, the p and dp/dt parameters in the Wilson program and a Wilson program means of generating eclipse timings from discovery and patrol based observations.

1. Introduction

Studies of contact binaries have led to very exciting results. This was recently highlighted by the discovery of Red Novae, characterized by a violent event which appears to be the final coalescence of the components of an over-contact binary into a fast rotating, blue straggler-like single star. The recovery of archived observations of a contact binary with high fill-out at the site of the red nova V1309 Sco (Tylenda *et al.* 2011; Tylenda and Kamiński 2016) has underscored the need for the characterization and continued patrol of such binaries in transition. The color of these objects distinguishes them from the usually blue, high temperature novae and supernovae. Archival data indicate that other similar events have happened in the past, with V838 Mon (Bond *et al.* 2003) and M31-RV (Boschi and Munari 2004) as examples.

Other interesting results have been determined in the past years. For instance, many contact binaries are found to be a part of triple and multiple star systems. Chambliss noticed this fact (1992). This may give insight into their origins. Kinematics, and the high abundance of contact binaries, gives hints about their old age (Guinan and Bradstreet 1988). Oscillations of all amplitudes are common and are not only attributed to their orbits in triple star systems, but their magnetic cycles (Han *et al.* 2019). Also, continuous positive or negative period changes about near contact configurations may be due to Thermal Relaxations Oscillations (TRO; Lucy 1976; Flannery 1976; Robertson and Eggleton 1977). The TRO model explains that the binary configuration undergoes periodic oscillations between semidetached and contact configurations about a state of marginal contact. In the broken contact phase, the mass ratio (q) increases and the period decreases. In the contact phase q decreases and period increases. All of these results point to the importance of observations of contact and near contact systems. PY Aquarii is another of these interesting eclipsing binaries whose photometric study is summarized in the next few paragraphs.

PY Aqr (GSC 05191-00853, 2MASS J20535602−0632016, V = 12.7–13.3 mag) was discovered in 2003 by observers C. Demeautis, D. Matter, and V. Cotrez (Demeautis *et al.* 2005). The system is listed as Object No. 77 in "Reports of New Discoveries No. 17" (Olah and Jurcsik 2005), which gives an EW type and contains links to a finding chart, a figure of the light curve, and a light curve data file with ephemeris:

$$\text{HJD(min)} = 2452877.558\text{d} + 0.40210 \times \text{E}. \quad (1)$$

The variable was also observed by the All Sky Automated Survey (Pojmański 2002) and is listed as ASAS J205356−0632.1 in the ASAS-3 data file. The binary received the name PY Aqr in the "80th Name List of Variable Stars" (Kazarovets *et al.* 2013). The new GAIA DR2 (Riello *et al.* 2018) results give a distance of 605 ±14 pc.

PY Aqr is a solar-type contact binary and since it is moderately bright and totally eclipsing, it is easily monitored with small telescopes. A preliminary study of PY Aqr was presented at the AAS meeting #231 (Chamberlain *et al.* 2018). A more complete photometric study and period analysis are presented here.

2. New photometry and data reduction

Light curves in *B*, *V*, *R*, and *I* were obtained with the 0.6-m SARA South reflector at Cerro Tololo Inter-American Observatory in remote mode on 17 July, 17 August, 23 September, and 17 October, 2017. The telescope was equipped

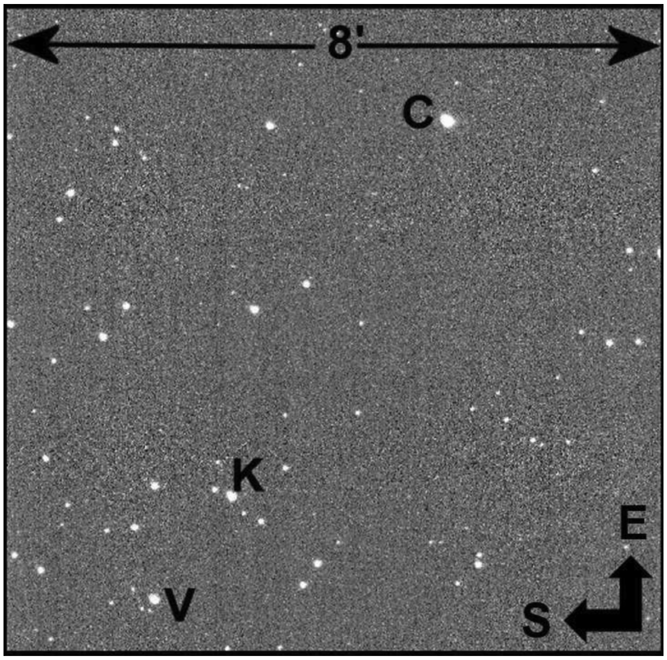

Figure 1. PY Aqr (V), comparison star C (2MASS J2054027−0630586), and check star K (2MASS J205356024−0632016).

with a thermoelectrically cooled (−38° C) 1 K × 1 K pixel FLI camera and Bessell *BVRI* filters. We obtained 111 individual observations in *B*, 136 in *V*, 131 in *R*, and 128 in *I*. The standard error of a single observation was 10 mmag in *B*, *R*, and *I*, and 12 mmag in *V*. The finding chart, given here for future observers, is shown in Figure 1. Characteristics of the variable, comparison, and check star are listed in Table 1.

The C–K magnitude differences remained constant throughout the observing run to better than 1%. Exposure times varied from 200–250 s in *B*, 100–140 s in *V*, and 30–75 s in *R* and *I*. Nightly images were calibrated with 25 bias frames, at least five flat frames in each filter, and ten 350-second dark frames. The light curve data are listed in Table 2. Light curve amplitudes and the differences in magnitudes at various quadratures are given in Table 3. Curve-dependent σs used in the Wilson program are given in Table 4. The new curves are of good precision, about 1% photometric precision.

The amplitude of the light curve varies from 0.61 to 0.53 magnitude in *B* to *I*. The O'Connell effect, an indicator of spot activity, averages several times the noise level, 0.02–0.04 mag, indicating magnetic activity. The differences in minima are small, 0.02–0.04 mag, indicating over-contact light curves in good thermal contact. A time of constant light appears to occur at minima and lasts some 23 minutes as measured by the light curve solution about phase 0.5.

3. Light curve solution

The new *B*, *V*, R, and I light curves were pre-modeled with BINARY MAKER 3.0 (Bradsteet and Steelman 2002), with each curve fitted separately. Each yielded an over-contact binary configuration. Averaged parameters were then used as starting values for a solution by the method of differential corrections (DC) using the Wilson-Devinney (WD) binary star program (Wilson and Devinney 1971; Wilson 1979) and revised several times, most recently as described in Wilson and Van Hamme (2014). To increase the time baseline and improve the determination of ephemeris parameters, including a period rate of change, the new multiband light curves were combined with the 2003 discovery light curve in Olah and Jurcsik (2005) and the ASAS light curve in the ASAS-3 database.

The 2MASS catalog lists a color *J–K* color of 0.384 ± 0.033, which is consistent with a primary component of solar spectral type (Houdashelt, Bell, and Sweigart 2000; Cox 2000). Accordingly, a surface temperature of 5750 K was adopted for the primary component mean surface temperature. Limb darkening coefficients were interpolated locally in terms of surface temperature and gravity in the tables of Van Hamme (1993) for a logarithmic law. The detailed reflection effect treatment with one reflection (Wilson 1990) was selected. The solution was run in mode 3 (over-contact) with convective values for the gravity brightening parameters ($g1 = g2 = 0.32$) and albedos ($A1 = A2 = 0.5$).

Essential information on light curve weighting is in Wilson (1979), including a discussion of level-dependent, curve-dependent, and individual data point weights. Level-dependent weights for the light curves were generated within the DC program assuming photon counting statistics. For individual data point weights, only weight ratios matter among the points of a given data subset. Accordingly, the scaling factor for individual weights can be set arbitrarily. Here, individual light curve points were given unit weights. Curve-dependent weights (Table 3) were based on fixed σs computed by the DC program.

Solution parameters are listed in Table 5. Solution 1 includes a period rate of change as one of the adjusted parameters, whereas Solution 2 does not include a dP/dt. Note that the orbit semi-major axis (a) is not a solution parameter since no radial velocities for the system exist. The Table 5 value of a is the adopted value that produces a primary mass close to that of the Sun. Light and Solution 1 curves vs. orbit phase are shown in Figures 2 and 3, and, for selected nights, vs. time in Figures 4 to 7. Figure 8 is the V plot with Solution 1 less the dark spot to show the effects of it. The spot affects the curve from phase 0.6 to phase 0.1.

Table 1. Photometric targets.

Role	*Label*	*Name*	*V*	*J−K*
Variable	V	PY Aqr	12.72–13.37	0.384 ± 0.033
Comparison	C	TYC 5191-971-1	11.51	0.313 ± 0.035
Check	K	2MASS J20540271−0630486	12.73	0.632 ± 0.033

Note: The C−K magnitude differences remained constant throughout the observing run to better than 1%. Exposure times varied: 200–250 s in B, 100–140 s in V, and 30–75 s in R and I. Nightly images were calibrated with 25 bias frames, at least five flat frames in each filter, and ten 350-second dark frames. The light curve data are listed in Table 2.

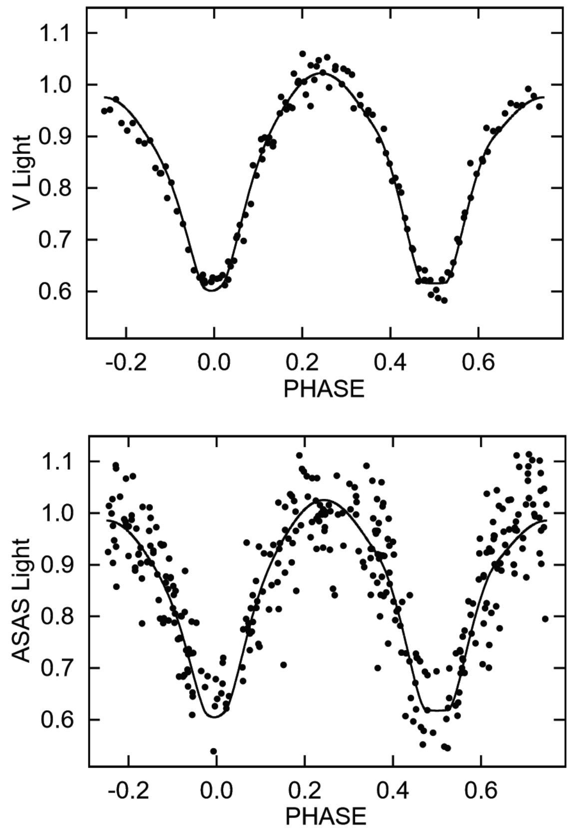

Figure 2. The PY Aqr 2003 (upper panel) and ASAS (lower panel) observed and Solution 1 computed light curves phased with the orbit period. Light units are normalized flux.

Light curve asymmetries were modeled with spots as described in Wilson (2012). The WD program allows for different spot configurations at different epochs, and this feature was exploited here. Times of onset and end of each of the intervals of spot growth, maximum, and decay are included in Table 5.

An eclipse duration of ~22 minutes was determined for the secondary eclipse (phase 0.5) from the light curve solution. The fill-out is ~18%, indicating a modest degree of over-contact. Fill-out is defined as:

$$\text{fill-out} = \frac{\Omega_1 - \Omega_{ph}}{\Omega_1 - \Omega_2} \quad (2)$$

where Ω_1 is the inner critical potential where the Roche Lobe surfaces reach contact at L_1, and Ω_2 is the outer critical potential where the surface reaches L_2.

The more massive component has a lower temperature, characteristic of a W-type (smaller component is hotter) W UMa system. This conclusion is not very firm, however. We will have to await spectroscopic observations and the determination of radial velocities before the W-type nature of the binary can be confirmed. Although photometric mass ratios for totally eclipsing over-contact binaries are reliable (see e.g. Terrell and Wilson 2005), spot effects in PY Aqr are not fully modeled, as indicated by night-to-night variations in light curve shapes (Figures 4 to 7). Radial velocities will be needed to pin down the mass ratio and determine absolute dimensions.

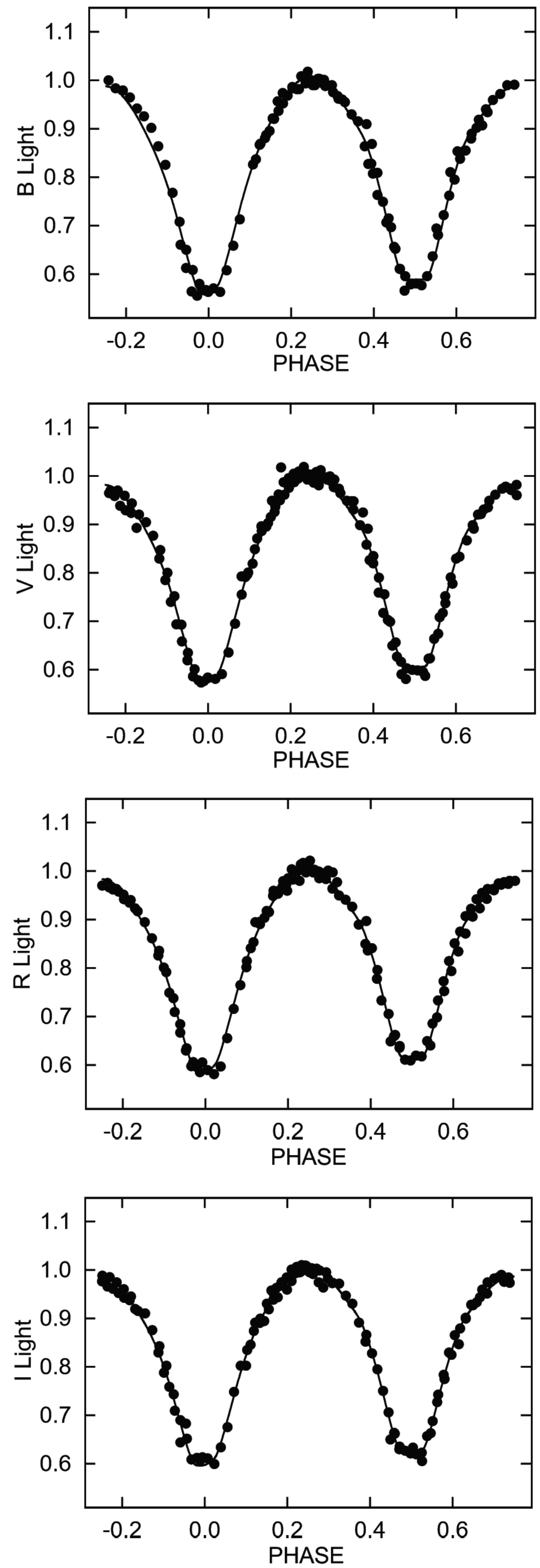

Figure 3. The PY Aqr 2017 observed and Solution 1 computed light curves phased with the orbit period. Light units are normalized flux.

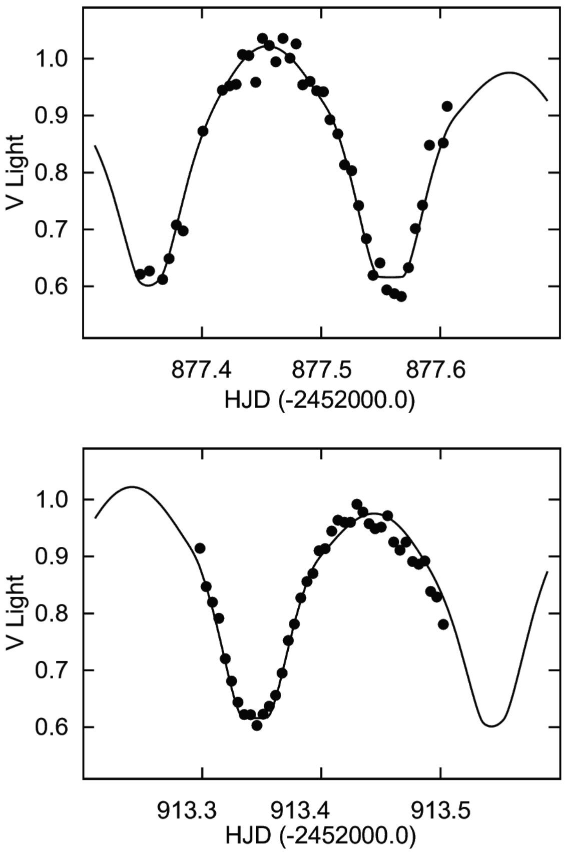

Figure 4. The PY Aqr 2003 August 25 (upper panel) and September 30 (lower panel) observed and Solution 1 computed light curves. Light units are normalized flux.

4. Orbit period and ephemerides

Solving the light curves with time (and not phase) as the independent variable allows adjustment of ephemeris parameters, which are then determined from whole light curves and not just timing minima (see e.g. Van Hamme and Wilson 2007). Solutions 2 and 1, respectively, yield linear and quadratic ephemerides:

$$\mathrm{HJD(min)} = 2455460.00294 \pm 0.00034 + 0.402093519 \pm 0.000000051 \times \mathrm{E}, \quad (3)$$

and

$$\mathrm{HJD(min)} = 2455459.9909 \pm 0.0013 + 0.402093472 \pm 0.000000048 \times \mathrm{E} + 3.10 \pm 0.32 \times 10^{-10} \times \mathrm{E}^2, \quad (4)$$

with the coefficient of the E^2 term derived from the Solution 1 dP/dt value. The photometric data span an interval of about 16 years and show an orbital period that is increasing at a rate dP/dt $= +1.54 \pm 0.16 \times 10^{-9}$. Formally, the quadratic term is significant, having a value of 9 times its standard deviation. However, we should be cautious and not over-interpret this result. Information on dP/dt comes predominantly from six eclipses, four which occur in 2003 at the beginning of the 16-year span and two in 2017 at the end. Because of the low frequency of ASAS observations (one data point every one or two days), that light curve contains no eclipses with full phase coverage. However, there are a fair number of ingress and egress points in the ASAS

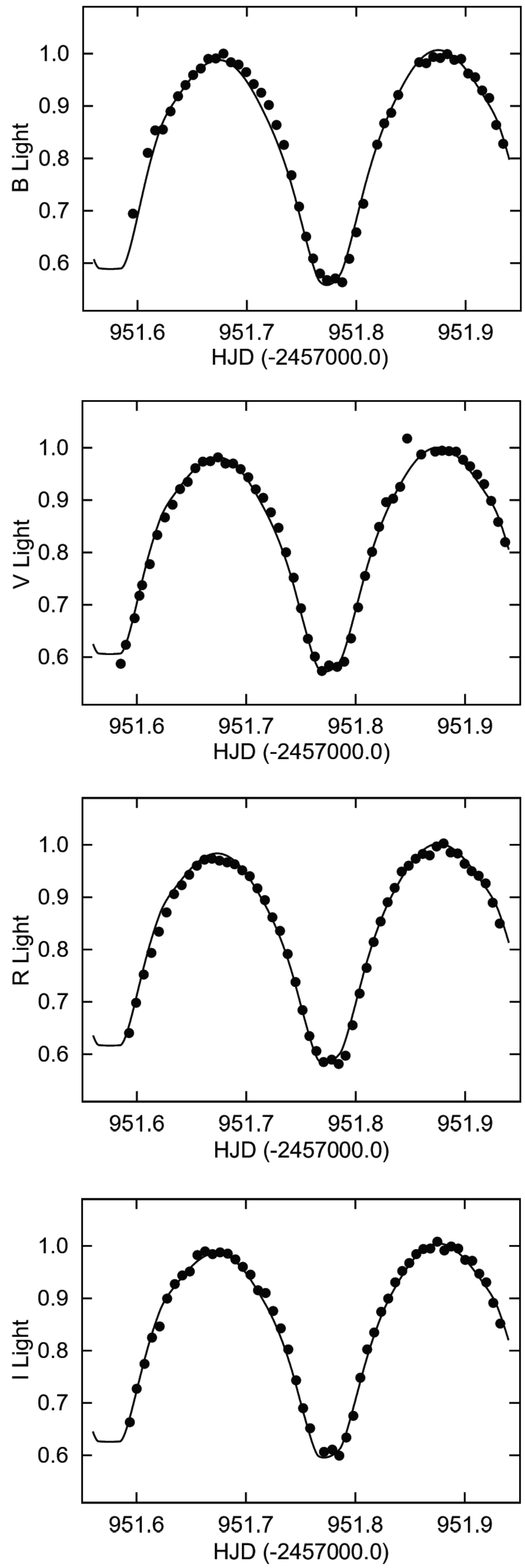

Figure 5. The PY Aqr July 17, 2017 observed and Solution 1 computed light curves. Light units are normalized flux.

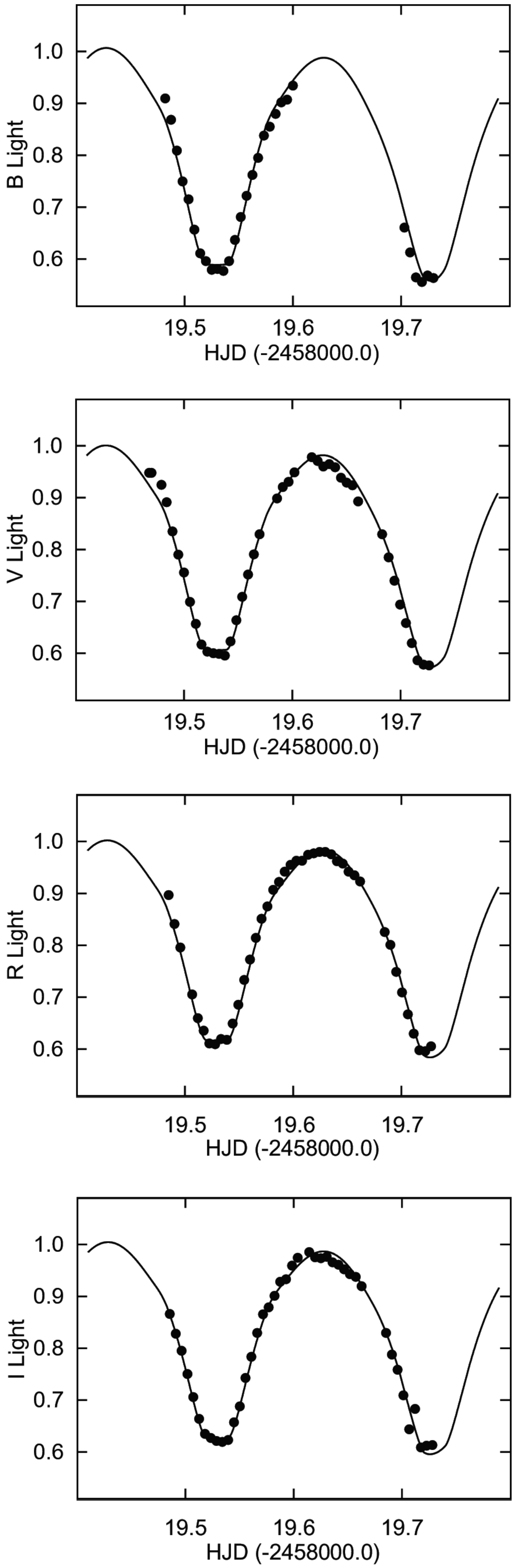

Figure 6. The PY Aqr September 23, 2017 observed and Solution 1 computed light curves.

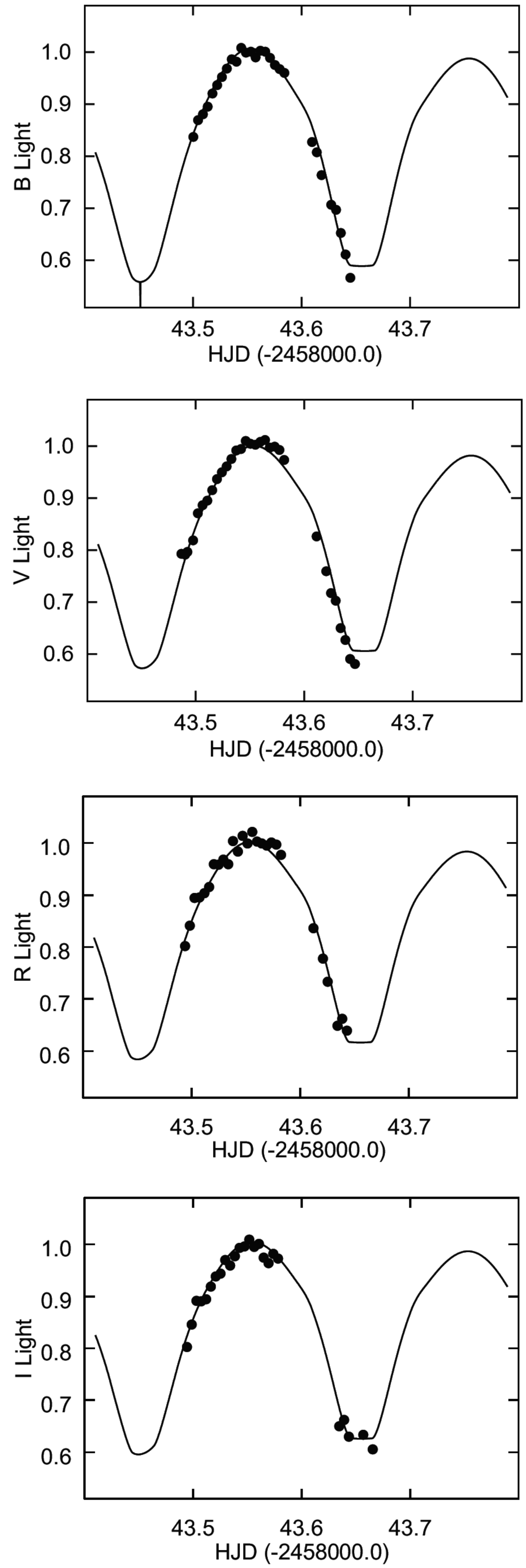

Figure 7. The PY Aqr October 17, 2017 observed and Solution 1 computed light curves. Light units are normalized flux.

curve which help determine the value of dP/dt. Unfortunately, the lack of observational data between 2009 and 2017 represents a significant gap in the 16-year time base of Equation 3, and the significance of the quadratic term is solely due to the new 2017 light curve data. Futures light curves or times of mid-eclipse are needed to confirm the dP/dt derived here.

For the purpose of future period studies, we extracted individual eclipse timings from the various data sets in the following manner. For eclipses with full phase coverage (four in the 2003 light curve and two in the 2017 curves), we used the DC program to fit single-night sections of curves that contain the eclipse, selecting an initial zero-epoch value near mid-eclipse, and then adjusting the zero-epoch T_0 and luminosity L_1 (to set the light level) only, keeping all other parameters fixed at global solution values. The final zero-epoch time marks a time of conjunction of the two stars that night, and hence, a time of mid-eclipse. For the ASAS light curve with its sparse phase coverage, full eclipses are not available. However, we can identify light curve sections spanning about 200 to 300 days that have at least a few points in or near an eclipse, select an initial zero-epoch near those points, and apply DC to determine the time of conjunction closest to those points from the entire light curve section. As expected, such eclipse timings will have larger errors, but properly weighted they will be useful in future period analyses.

We obtained a total of 15 eclipse timings. They are listed in Table 6 together with their standard errors and eclipse type (primary or secondary). Least-squares fits (weighted, with relative weights inversely proportional to the standard errors squared) yield ephemerides:

$$\mathrm{HJD(min)} = 2455460.00291 \pm 0.00078 + 0.40209363 \pm 0.000000012 \times E, \quad (5)$$

and

$$\mathrm{HJD(min)} = 2455459.9903 \pm 0.0028 + 0.402093617 \pm 0.000000078 \times E + 3.27 \pm 0.71 \times 10^{-10} \times E^2, \quad (6)$$

which corresponds to a dP/dt of $1.63 \pm 0.35 \times 10^{-9}$, in excellent agreement with the dP/dt in Table 4 determined from the whole light curves. Figure 9 shows timing residuals with respect to Eqn. 4 and a fitted quadratic curve. Clearly, the significance of the quadratic term is solely due to the two 2017 eclipse times. Table 5 minima can be combined with future eclipse timings to monitor the period behavior of the system.

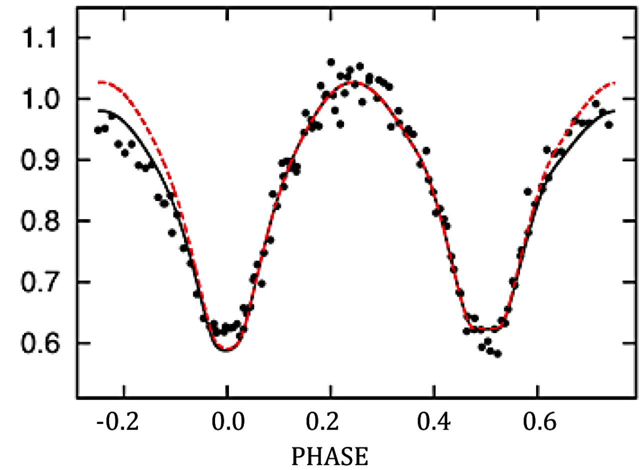

Figure 8. The PY Aqr 2017 V-observed and Solution 1 (see Figure 3) computed light curve phased with the orbit period and the synthetic curve less the dark spot (red dashed line). Light units are normalized flux.

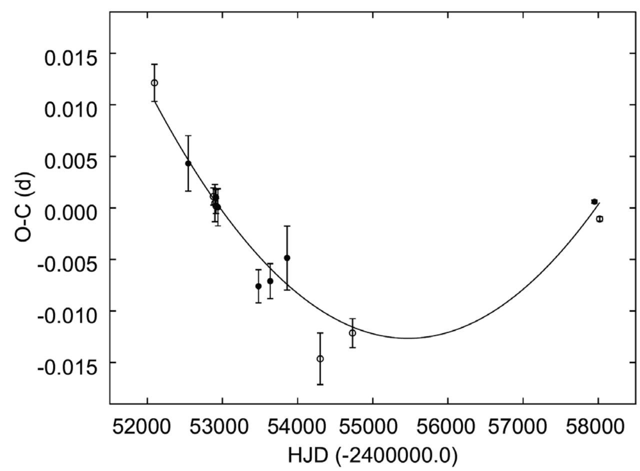

Figure 9. PY Aqr eclipse timing residuals (Equation 4) and quadratic fit. Filled and open circles indicate primary and secondary timings, respectively.

5. Discussion

PY Aqr is an over-contact W UMa in possibly a W-type configuration ($T_2 > T_1$). The system has a mass ratio of ~0.34, and a component temperature difference of only ~40 K. One cool region of spots (Tfact ~ 0.64, ~33-degree radius) was iterated on the primary component in the WD Synthetic Light Curve computations for the new photometry. This temperature is quite normal for average spot temperatures on the Sun (T ~ 4660). It appears in the Southern hemisphere (colatitude 138 degrees). The Roche Lobe fill-out of the binary is only ~10% with an inclination of ~82°, high enough for total eclipses. Its spectral type indicates a surface temperature of ~5750 K for the primary component, making it a solar-type binary. Such a main sequence star would have a mass of ~0.92 $M_\odot$ and the secondary (from the mass ratio) would have a mass of 0.32 $M_\odot$, making it very much undersized. The W-type phenomena may to be due to saturation of magnetic phenomena on the primary component, suppressing its temperature. The secondary component, which is probably near that of the actual temperature of the primary, has a temperature of ~5800 K.

6. Conclusions

The steady period increase does not support the idea of a red nova precursor status for PY Aqr. Such a status would be characterized by a decreasing period at an increasingly rapid rate, shrinking the orbit and leading to a Darwin instability and merger of the two stars (see e.g. Tylenda *et al.* 2011). The phenomenon of long-term increase in the orbital period can be explained by the mass transfer from the less massive component to the more massive component (Qian 2001a, 2001b), which agrees with the TRO theory. The positive quadratic period increase would indicate a mass exchange rate of

$$\frac{dM}{dt} = \frac{\dot{P} M_1 M_2}{3P (M_1 - M_2)} \sim \frac{1.8 \times 10^{-7} M_\odot}{d}. \quad (7)$$

with the primary component being the gainer. However, the period change might point to another possibility. The period increase might be a part of a sinusoidal oscillation, meaning that there is a third body orbiting the system. Alternately, if magnetic braking is also acting (which is likely), the fill-out will be moderated and the components may not separate. A steadily decreasing mass ratio would ultimately lead to an unstable condition and the possible coalescence of the binary. This all points to the need of further efforts to monitor the system for times of mid-eclipse to determine the nature of the orbital evolution. Otherwise, the stars are in fair thermal contact. Obtaining radial velocities will be the next step towards determining astrophysically relevant parameters of the PY Aqr system.

7. Acknowledgements

We thank the Southeastern Association for Research in Astronomy for time on the CTIO SARA telescope. We made use of the SIMBAD database, operated at the CDS, Strasbourg, France. This work has made use of data from the European Space Agency (ESA) mission Gaia (https://www.cosmos.esa.int/gaia), processed by the Gaia Data Processing and Analysis Consortium (DPAC; https://www.cosmos.esa.int/web/gaia/dpac/consortium). Funding for the DPAC has been provided by national institutions, in particular the institutions participating in the Gaia Multilateral Agreement.

References

Bond, H. E., *et al.* 2003, *Nature*, **422**, 405.

Boschi, F., and Munari. U. 2004, *Astron. Astrophys.*, **418**, 869.

Bradstreet, D. H., and Steelman, D. P. 2002, *Bull. Amer. Astron. Soc.*, **34**, 1224.

Chamberlain, H., Samec, R. G., Caton, D. B., and Van Hamme, W. 2018, Amer. Astron. Soc. Meeting #231, 434.03.

Chambliss, Carlson R. 1992, *Publ. Astron. Soc. Pacific*, **104**, 663.

Cox, A. N. 2000, *Allen's Astrophysical Quantities*, 4th ed. AIP Press/Springer, New York.

Demeautis, C., Matter, D., Cotrez, V., Behrend, R., and Rinner, C. 2005, *Inf. Bull. Var. Stars*, No. 5600, 15.

Flannery, B. P. 1976, *Astrophys. J.*, **205**, 217.

Guinan, E. F., and Bradstreet, D. H. 1988, in *Formation and Evolution of Low Mass Stars*, eds. A. K. Dupree, and M. T. V. T. Lago, NATO Adv. Sci. Inst. Ser. C, Vol. 241, Kluwer, Dordrecht, 345.

Han, Q.-w., Li, L.-f., Kong, X.-y., Li, J.-s., and Jiang, D.-k. 2019, *New Astron.*, **66**, 14.

Houdashelt, M. L., Bell, R. A., and Sweigart, A. V. 2000, *Astron. J.*, **119**, 1448.

Kazarovets, E. V., Samus, N. N., Durlevich, O. V., Kireeva, N. N., and Pastukhova, E. N. 2013, *Inf. Bull. Var. Stars*, No. 6052, 1.

Lucy L. B., 1976, *Astrophys. J.*, **205**, 208.

Olah, K., and Jurcsik, J., eds. 2005, *Inf. Bull. Var. Stars*, No. 5600, 1.

Pojmański, G. 2002, *Acta Astron.*, **52**, 397.

Qian, S. 2001a, *Mon. Not. Roy. Astron. Soc.*, **328**, 635.

Qian, S. 2001b, *Mon. Not. Roy. Astron. Soc.*, **328**, 914.

Robertson J. A., and Eggleton P. P., 1977, *Mon. Not. Roy. Astron. Soc.*, 179, 359.

Riello, M., *et al.* 2018, Gaia Data Release 2: Processing of the photometric data, *Astron. Astrophys.*, **616**, id.A4 (arXiv:1804.09368).

Terrell, D., and Wilson, R. E. 2005, *Astrophys. Space Sci.*, **296**, 221.

Tylenda, R., and Kamiński, T. 2016, *Astron. Astrophys.*, **592A**, 134.

Tylenda, R., *et al.* 2011, *Astron. Astrophys.*, **528A**, 114.

Van Hamme, W. 1993, *Astron. J.*, **106**, 2096.

Van Hamme, W., and Wilson, R. E. 2007, *Astrophys. J.*, **661**, 1129.

Wilson, R. E. 1979, *Astrophys. J.*, **234**, 1054.

Wilson, R. E. 1990, *Astrophys. J.*, **356**, 613.

Wilson, R. E. 2012, *Astron. J.*, **144**, 73.

Wilson, R. E., and Devinney, E. J. 1971, *Astrophys. J.*, **166**, 605.

Wilson, R. E., and Van Hamme, W. 2014, *Astrophys. J.*, **780**, 151.

Table 2. PY Aqr: new *BVRI* photometry (variable minus TYC 5191-971-1, the comparison star).

HJD 2457000+	ΔB	*HJD* 2457000+	ΔB	*HJD* 2457000+	ΔB	*HJD* 2457000+	ΔB	*HJD* 2457000+	ΔB
51.5957	1.836	51.7605	1.979	51.9280	1.599	119.5626	1.735	143.5400	1.460
51.6093	1.668	51.7669	2.031	51.9344	1.645	119.5679	1.689	143.5444	1.431
51.6162	1.612	51.7733	2.055	82.8047	1.488	119.5733	1.632	143.5488	1.441
51.6232	1.610	51.7808	2.049	82.8096	1.469	119.5786	1.610	143.5533	1.439
51.6301	1.567	51.7872	2.063	82.8340	1.421	119.5840	1.579	143.5577	1.451
51.6370	1.532	51.7936	1.980	82.8389	1.451	119.5893	1.552	143.5621	1.437
51.6439	1.507	51.8000	1.893	82.8438	1.437	119.5947	1.546	143.5665	1.439
51.6508	1.485	51.8064	1.807	82.8487	1.447	119.6000	1.514	143.5710	1.452
51.6578	1.471	51.8192	1.647	119.4821	1.543	119.7031	1.890	143.5754	1.467
51.6647	1.451	51.8256	1.595	119.4874	1.593	119.7084	1.972	143.5798	1.476
51.6716	1.450	51.8320	1.570	119.4928	1.670	119.7138	2.061	143.5842	1.484
51.6785	1.440	51.8384	1.529	119.4981	1.753	119.7192	2.078	143.6097	1.646
51.6854	1.458	51.8576	1.458	119.5036	1.804	119.7245	2.054	143.6141	1.672
51.6924	1.463	51.8640	1.460	119.5090	1.897	119.7299	2.063	143.6185	1.733
51.6993	1.479	51.8704	1.447	119.5144	1.975	143.5002	1.633	143.6273	1.817
51.7062	1.505	51.8768	1.449	119.5197	2.002	143.5046	1.592	143.6318	1.832
51.7131	1.524	51.8832	1.441	119.5251	2.033	143.5091	1.578	143.6362	1.904
51.7201	1.552	51.8896	1.453	119.5304	2.030	143.5135	1.560	143.6406	1.975
51.7270	1.599	51.8960	1.451	119.5358	2.037	143.5179	1.530	143.6450	2.058
51.7339	1.648	51.9024	1.482	119.5411	2.002	143.5223	1.511		
51.7408	1.727	51.9088	1.490	119.5465	1.930	143.5267	1.493		
51.7477	1.815	51.9152	1.519	119.5518	1.857	143.5311	1.475		
51.7541	1.907	51.9216	1.536	119.5572	1.794	143.5356	1.455		

HJD 2457000+	ΔV	*HJD* 2457000+	ΔV	*HJD* 2457000+	ΔV	*HJD* 2457000+	ΔV	*HJD* 2457000+	ΔV
51.5853	1.898	51.7692	1.924	82.8160	1.325	119.5912	1.410	143.5153	1.416
51.5899	1.833	51.7757	1.904	82.8208	1.315	119.5966	1.398	143.5197	1.391
51.5979	1.748	51.7831	1.909	82.8257	1.310	119.6020	1.377	143.5241	1.376
51.6023	1.681	51.7895	1.891	82.8306	1.300	119.6180	1.344	143.5285	1.363
51.6048	1.651	51.7959	1.812	82.8355	1.319	119.6234	1.352	143.5329	1.347
51.6118	1.593	51.8023	1.715	82.8404	1.335	119.6287	1.364	143.5374	1.329
51.6187	1.518	51.8087	1.625	82.8453	1.341	119.6341	1.359	143.5418	1.326
51.6257	1.475	51.8151	1.561	119.4677	1.378	119.6395	1.366	143.5462	1.309
51.6326	1.445	51.8215	1.498	119.4700	1.378	119.6449	1.389	143.5506	1.315
51.6395	1.409	51.8279	1.439	119.4791	1.405	119.6502	1.400	143.5551	1.317
51.6464	1.393	51.8343	1.431	119.4839	1.445	119.6556	1.406	143.5595	1.311
51.6534	1.363	51.8407	1.404	119.4893	1.516	119.6609	1.443	143.5639	1.307
51.6603	1.349	51.8471	1.301	119.4947	1.576	119.6830	1.523	143.5683	1.323
51.6672	1.348	51.8599	1.334	119.5000	1.624	119.6889	1.583	143.5728	1.321
51.6741	1.340	51.8727	1.328	119.5055	1.709	119.6943	1.647	143.5772	1.328
51.6810	1.353	51.8791	1.326	119.5109	1.777	119.6996	1.717	143.5816	1.349
51.6880	1.353	51.8855	1.327	119.5162	1.845	119.7050	1.774	143.6115	1.527
51.6949	1.365	51.8919	1.328	119.5216	1.869	119.7104	1.840	143.6203	1.619
51.7018	1.383	51.8983	1.345	119.5270	1.875	119.7157	1.900	143.6247	1.681
51.7087	1.410	51.9047	1.359	119.5323	1.877	119.7211	1.915	143.6291	1.703
51.7156	1.429	51.9111	1.377	119.5377	1.883	119.7264	1.918	143.6336	1.788
51.7226	1.463	51.9175	1.398	119.5430	1.834	143.4868	1.572	143.6380	1.827
51.7295	1.500	51.9239	1.436	119.5484	1.765	143.4904	1.574	143.6424	1.892
51.7364	1.562	51.9303	1.486	119.5538	1.694	143.4924	1.567	143.6468	1.910
51.7433	1.630	51.9367	1.536	119.5591	1.630	143.4976	1.537		
51.7500	1.718	82.7997	1.377	119.5645	1.575	143.5020	1.470		
51.7564	1.813	82.8062	1.362	119.5698	1.523	143.5064	1.451		
51.7628	1.873	82.8111	1.334	119.5859	1.436	143.5108	1.440		

Table continued on next page

Table 2. PY Aqr: new *BVRI* photometry (ariable minus TYC 5191-971-1, the comparison star), cont.

HJD *2457000+*	ΔR_c	*HJD* *2457000+*	ΔR_c	*HJD* *2457000+*	ΔR_c	*HJD* *2457000+*	ΔR_c	*HJD* *2457000+*	ΔR_c
51.5929	1.744	51.7780	1.834	82.8131	1.283	119.5922	1.325	143.5117	1.370
51.5993	1.650	51.7844	1.849	82.8180	1.276	119.5976	1.310	143.5161	1.356
51.6063	1.569	51.7908	1.820	82.8229	1.273	119.6030	1.301	143.5205	1.305
51.6132	1.511	51.7972	1.719	82.8278	1.259	119.6083	1.301	143.5249	1.306
51.6201	1.457	51.8036	1.623	82.8326	1.242	119.6137	1.288	143.5293	1.295
51.6271	1.410	51.8100	1.551	82.8375	1.250	119.6190	1.285	143.5338	1.305
51.6340	1.367	51.8164	1.483	82.8424	1.263	119.6244	1.282	143.5382	1.256
51.6409	1.347	51.8228	1.432	82.8473	1.264	119.6297	1.282	143.5426	1.278
51.6478	1.324	51.8292	1.386	119.4849	1.378	119.6352	1.287	143.5470	1.245
51.6547	1.304	51.8356	1.353	119.4903	1.448	119.6405	1.302	143.5515	1.261
51.6617	1.291	51.8420	1.317	119.4957	1.508	119.6459	1.307	143.5559	1.237
51.6686	1.289	51.8484	1.304	119.5066	1.639	119.6512	1.325	143.5603	1.257
51.6755	1.293	51.8548	1.289	119.5119	1.712	119.6566	1.333	143.5647	1.261
51.6824	1.297	51.8612	1.279	119.5173	1.752	119.6619	1.347	143.5692	1.265
51.6893	1.301	51.8676	1.282	119.5226	1.795	119.6846	1.468	143.5736	1.259
51.6963	1.314	51.8740	1.263	119.5280	1.798	119.6899	1.501	143.5780	1.263
51.7032	1.327	51.8804	1.257	119.5333	1.780	119.6953	1.574	143.5824	1.285
51.7101	1.354	51.8868	1.276	119.5387	1.783	119.7006	1.633	143.6123	1.454
51.7170	1.381	51.8932	1.278	119.5441	1.729	119.7060	1.700	143.6211	1.533
51.7239	1.422	51.8996	1.300	119.5494	1.670	119.7114	1.762	143.6255	1.597
51.7309	1.455	51.9060	1.316	119.5548	1.597	119.7167	1.819	143.6344	1.730
51.7378	1.514	51.9124	1.326	119.5601	1.540	119.7221	1.822	143.6388	1.708
51.7449	1.590	51.9188	1.343	119.5655	1.483	119.7274	1.805	143.6432	1.746
51.7514	1.672	51.9252	1.387	119.5708	1.435	143.4940	1.500		
51.7577	1.754	51.9316	1.437	119.5762	1.405	143.4984	1.448		
51.7641	1.804	82.8033	1.317	119.5815	1.366	143.5028	1.381		
51.7706	1.842	82.8082	1.312	119.5869	1.348	143.5072	1.380		

HJD *2457000+*	ΔI_c	*HJD* *2457000+*	ΔI_c	*HJD* *2457000+*	ΔI_c	*HJD* *2457000+*	ΔI_c	*HJD* *2457000+*	ΔI_c
51.5938	1.666	51.7789	1.755	82.8073	1.261	119.5769	1.360	143.4988	1.402
51.6002	1.566	51.7853	1.776	82.8122	1.248	119.5823	1.333	143.5032	1.345
51.6072	1.497	51.7917	1.715	82.8171	1.240	119.5876	1.301	143.5076	1.346
51.6141	1.429	51.7981	1.646	82.8220	1.219	119.5930	1.295	143.5121	1.341
51.6211	1.401	51.8045	1.535	82.8268	1.213	119.5984	1.265	143.5165	1.312
51.6280	1.335	51.8109	1.459	82.8317	1.209	119.6037	1.248	143.5209	1.289
51.6349	1.302	51.8173	1.416	82.8366	1.220	119.6144	1.236	143.5253	1.283
51.6418	1.283	51.8237	1.366	82.8415	1.216	119.6198	1.247	143.5297	1.253
51.6487	1.274	51.8301	1.335	82.8464	1.217	119.6251	1.249	143.5342	1.265
51.6557	1.239	51.8365	1.298	119.4856	1.376	119.6305	1.246	143.5386	1.245
51.6626	1.231	51.8429	1.273	119.4911	1.425	119.6359	1.258	143.5430	1.227
51.6695	1.237	51.8493	1.256	119.4964	1.469	119.6413	1.263	143.5475	1.224
51.6764	1.233	51.8557	1.237	119.5019	1.532	119.6466	1.273	143.5519	1.210
51.6834	1.236	51.8621	1.226	119.5073	1.598	119.6520	1.284	143.5563	1.225
51.6903	1.248	51.8685	1.225	119.5127	1.665	119.6573	1.290	143.5607	1.219
51.6972	1.264	51.8749	1.211	119.5180	1.713	119.6627	1.311	143.5651	1.248
51.7041	1.281	51.8813	1.229	119.5234	1.727	119.6853	1.423	143.5696	1.260
51.7110	1.316	51.8877	1.221	119.5287	1.737	119.6907	1.479	143.5740	1.240
51.7180	1.322	51.8941	1.225	119.5341	1.740	119.6960	1.520	143.5784	1.250
51.7249	1.364	51.9005	1.249	119.5395	1.734	119.7014	1.593	143.6348	1.688
51.7318	1.406	51.9069	1.251	119.5448	1.676	119.7067	1.698	143.6392	1.668
51.7387	1.459	51.9133	1.279	119.5502	1.626	119.7121	1.634	143.6436	1.722
51.7458	1.542	51.9197	1.298	119.5555	1.543	119.7175	1.759	143.6569	1.716
51.7522	1.623	51.9261	1.345	119.5609	1.485	119.7228	1.753	143.6657	1.765
51.7586	1.685	51.9325	1.394	119.5662	1.423	119.7282	1.751		
51.7714	1.763	82.8024	1.267	119.5716	1.377	143.4944	1.459		

Table 3. Averaged light curve characteristics of PY Aqr.

Filter	Phase	Magnitude Max. I	Phase	Magnitude Max. II
	0.25		0.75	
ΔB		1.441 ± 0.009		1.477 ± 0.025
ΔV		1.319 ± 0.011		1.355 ± 0.009
ΔR		1.253 ± 0.010		1.286 ± 0.005
ΔI		1.220 ± 0.007		1.241 ± 0.008
Filter	*Phase*	*Magnitude Min. II*	*Phase*	*Magnitude Max. I*
	0.50		0.00	
ΔB		2.033 ± 0.004		2.050 ± 0.012
ΔV		1.878 ± 0.004		1.914 ± 0.008
ΔR		1.789 ± 0.009		1.830 ± 0.017
ΔI		1.730 ± 0.011		1.748 ± 0.009
Filter		*Min. I – Max. I*		*Min. I – Min. II*
ΔB		0.609 ± 0.021		0.017 ± 0.015
ΔV		0.595 ± 0.019		0.036 ± 0.012
ΔR		0.577 ± 0.027		0.041 ± 0.026
ΔI		0.528 ± 0.016		0.018 ± 0.020
Filter		*Max. II – Max. I*		*Min. II– Max. I*
ΔB		0.036 ± 0.034		0.592 ± 0.013
ΔV		0.036 ± 0.020		0.559 ± 0.015
ΔR		0.033 ± 0.014		0.536 ± 0.018
ΔI		0.021 ± 0.015		0.510 ± 0.018

Table 4. Curve-dependent σs and data ranges.

Curve	Band	σ[a]	Range (HJD)
2003	V	0.0225	2452877.3–2452913.5
2017	B	0.0144	2457951.5–2458043.7
—	V	0.0160	—
—	R	0.0115	—
—	I	0.0105	—
ASAS	V	0.0683	2452025.8–2455144.6

Note a: In units of light at phase $0_p.25$.

Table 5. PY Aqr light curve solutions.

Parameter	Solution 1	Solution 2
a[a] ($R_\odot$)	2.52	2.52
i (deg)	83.57 ± 0.40	83.36 ± 0.44
T_1[b] (K)	5750	5750
T_2 (K)	5883 ± 16	5873 ± 17
Ω_1	2.483 ± 0.011	2.481 ± 0.011
Ω_2	2.48296	2.48138
Fill-out[c]	0.1870	0.1693
M_2/M_1	0.3249 ± 0.0045	0.3224 ± 0.0051
T_0 (HJD − 2455460.0)	−0.0091 ± 0.0013	0.00294 ± 0.00034
P0 (d)	0.402093472 ± 0.000000048	0.402093519 ± 0.000000051
dP/dt	+1.54 ± 0.16 × 10−9	—
$L_1/(L_1+L_2)V$	0.7107 ± 0.0037	0.7134 ± 0.0036
$L_1/(L_1+L_2)B$	0.7028 ± 0.0033	0.7058 ± 0.0035
$L_1/(L_1+L_2)V$	0.7107 ± 0.0028	0.7134 ± 0.0029
$L_1/(L_1+L_2)R$	0.7143 ± 0.0026	0.7171 ± 0.0027
$L_1/(L_1+L_2)I$	0.7170 ± 0.0026	0.7196 ± 0.0027
$L_1/(L_1+L_2)V$	0.7107 ± 0.0046	0.7134 ± 0.0048
χ^2	1.24	1.36
2003 Spot		
Co-latitude (deg)	109 ± 56	108 ± 114
Longitude (deg)	70.6 ± 8.5	73 ± 11
Radius (deg)	16 ± 24	16 ± 36
$T_{spot}/T_{surface}$	0.64 ± 2.4	0.70 ± 1.97
Time of Onset (HJD)	2451000	
Start of Maximum (HJD)	2452050	
End of Maximum (HJD)	2452950	
Time of Disappearance (HJD)	2457000	
2017 Spot		
Co-latitude (deg)	155.7 ± 5.9	154.7 ± 4.9
Longitude (deg)	21.5 ± 2.2	22.0 ± 2.3
Radius (deg)	36.0 ± 3.7	35.9 ± 3.4
$T_{spot}/T_{surface}$	0.693 ± 0.074	0.707 ± 0.065
Time of Onset (HJD)	2457000	
Start of Maximum (HJD)	2457950	
End of Maximum (HJD)	2458050	
Time of Disappearance (HJD)	2458500	
Auxiliary Parameters		
r_1(pole)	0.4549 ± 0.0015	0.4570 ± 0.0014
r_1(side)	0.4897 ± 0.0020	0.4922 ± 0.0018
r_1(back)	0.5185 ± 0.0022	0.5205 ± 0.0019
$\langle r_1 \rangle$d	0.4914 ± 0.0020	0.4911 ± 0.0017
r_2(pole)	0.2831 ± 0.0053	0.2763 ± 0.0056
r_2(side)	0.2969 ± 0.0066	0.2890 ± 0.0068
r_2(back)	0.3411 ± 0.0130	0.3290 ± 0.0129
$\langle r_2 \rangle$d	0.2982 ± 0.0017	0.2965 ± 0.0020

Notes: Band-specific parameters are listed in the order of Table3. a: Adopted to produce a primary star of mass ≈ $1M_\odot$. bBased on the color of the system. c: Defined as $(\Omega_{1,c} - \Omega_1)/(\Omega_{1,c} - \Omega_{2,c})$, with $\Omega_{1,c}$ and $\Omega_{2,c}$ the critical potentials at the L_1 and L_2 Lagrangian points, respectively. d: Radius of an equal-volume sphere.

Table 6. PY Aqr eclipse timings.

Timing (HJD)	*Error (d)*	*Type*	*Weight*[a]	*Source*[b]
2452094.6924	0.0018	2	0.309	ASAS
2452545.2305	0.0027	1	0.137	ASAS
2452877.55768	0.00083	2	1.45	IBVS
2452898.8680	0.0018	2	0.309	ASAS
2452908.31772	0.00083	1	1.45	IBVS
2452912.33873	0.00074	1	1.83	IBVS
2452913.34309	0.00073	2	1.88	IBVS
2452940.0822	0.0018	1	0.309	ASAS
2453478.8800	0.0016	1	0.391	ASAS
2453636.0991	0.0017	1	0.346	ASAS
2453860.0675	0.0031	1	0.104	ASAS
2454300.1492	0.0025	2	0.160	ASAS
2454729.5877	0.0014	2	0.510	ASAS
2457951.77773	0.00015	1	44.4	This paper
2458019.52884	0.00022	2	20.7	This paper

Notes: a. Relative weights, inversely proportional to the standard errors. b. Origin of light curves from which timings were extracted. IBVS refers to the 2003 light curve available from IBVS 5600 (Olah and Jurcsik 2005); ASAS (Pojmański 2002).